Sensors and Materials, Vol. 32, No. 2 (2020) 475–485
MYU Tokyo

S & M 2115

Linear-range Extension for Linear Variable Differential Transformer Using Binomial Series

Wandee Petchmaneelumka, Kanoknuch Songsuwankit,*
Jakkapun Tongcharoen, and Vanchai Riewruja

Department of Instrumentation and Control Engineering, Faculty of Engineering,
King Mongkut's Institute of Technology Ladkrabang, Bangkok, 10520, Thailand

(Received April 11, 2019; accepted December 23, 2019)

Keywords: linear variable differential transformer, inductive transducer, linear range extension, binomial series, operational amplifier, analog multiplier

The linear-range extension technique for a linear variable differential transformer (LVDT) is described in this paper. Generally, the LVDT has a narrow linear operating range caused by its nonlinear transfer characteristic. To extend the linear operating range, the nonlinear behavior of the LVDT must be adjusted. In this paper, the circuit building block providing the LVDT inverse transfer characteristic using binomial series approximation is proposed for linearizing the nonlinear behavior of the LVDT. The third-order inverse transfer characteristic of the LVDT is synthesized from analog multipliers and a difference amplifier comprising an operational amplifier (opamp). All active devices used in this study are commercially available. Therefore, the attraction of the proposed technique is in the simple configuration and low cost, making it suitable for an embedded measurement system. The performance of the proposed technique is discussed in detail. Simulation and experimental results confirming the performance are also included. As a result, the linear range of the commercial LVDT used in this study can be extended more than 500%. The full scale error of the measured value is about 0.23% over the entire operating range.

1. Introduction

An inductive transducer named the linear variable differential transformer (LVDT) provides the advantages of high resolution and durability.[1–3] The LVDT is used in applications to measure displacement, which can be observed in the engineering, industrial, automotive, military, robotic, scientific, and medical equipment fields.[1–11] The operation of the LVDT is based on the same principle as the transformer, which comprises a primary winding and two secondary windings with a moving core.[12,13] The output signal of the LVDT is the difference signal between two secondary winding signals. Therefore, the LVDT signal is directly proportional to the position of the moving core that can be used to measure the displacement with high resolution. When the excitation signal is applied to the primary

*Corresponding author: e-mail: kanoknuch.so@kmitl.ac.th
https://doi.org/10.18494/SAM.2020.2407

ISSN 0914-4935

winding of the LVDT, the secondary windings generate the LVDT output signal in the form of an amplitude modulation with suppressed carrier (AMSC).[13] Thus, the displacement signal can be extracted from the LVDT output signal using a synchronous demodulator based on a peak amplitude finder or an analog multiplier.[13–17] The transfer characteristic of the LVDT provides a nonlinear behavior for the moving core that varies in the maximum stroke range, which can be expressed as a third-order function of the core position.[2,12,18] Note that the linear operating range of the LVDT exists only in the narrow range close to the zero crossing. The large linear operating range of the LVDT with a compact structure is very useful for embedded measurement and instrumentation systems. However, the large linear operating range of the LVDT requires a large structure that is unsuitable for the embedded systems. In the past, the linear operating range of the LVDT was extended by the fractional order technique.[19] Unfortunately, this technique is suited to a special design of the LVDT that causes a complex and large structure. The technique based on an artificial neural network (ANN) has been introduced in the literature.[20,21] This technique can extend the linear operating range of the commercial LVDT using an adaptive inverse model. The use of the ANN technique requires a high-speed signal processor to calculate the adaptive inverse model. This is inconvenient for the embedded measurement system and uneconomical. Moreover, the ANN technique provides a large response time to obtain the linear displacement signal.

In this paper, the circuit building block providing the inverse transfer characteristic of the LVDT is proposed. The binomial series is used to estimate the inverse transfer characteristic of the LVDT. The LVDT output signal is demodulated to the displacement signal by the technique reported previously.[13] The displacement signal is compensated to the linear displacement signal by the proposed scheme. Note that the proposed scheme can be implemented using only commercially available devices. The performance of the proposed technique is analyzed and discussed in detail. Experimental results show that the maximum percentage error of about 0.5% in the maximum stroke range is observed. The linear operating range of the commercial LVDT can be extended more than 500% by using the proposed technique. It is clearly seen that the proposed technique exhibits the advantages of fast response, high accuracy, simple configuration, and low cost.

2. Basic Principle of LVDT

The LVDT principle is similar to that of a transformer that comprises a primary winding P, two identical secondary windings, S_1 and S_2, and a moving core, as shown in Fig. 1(a). Two secondary windings are connected in opposed directions to generate the displacement signal. The amplitude of the displacement signal versus the core position is shown in Fig. 1(b). The structure of the LVDT is shown in Fig. 1(c), where the lengths of the primary winding and secondary windings are defined as p and w, respectively, with the radius d_O. The number of turns in the primary winding and secondary windings are equal to n_p and n_s, respectively. The dimensions of the LVDT core are obtained as the radius d_C and length L_C. The insulators between the primary winding and the secondary windings have a thickness of g. The sinusoidal signal $v_{ex} = V_{ex}\sin(\omega_{ex}t)$ is applied as the excitation signal for the primary winding, where V_{ex}

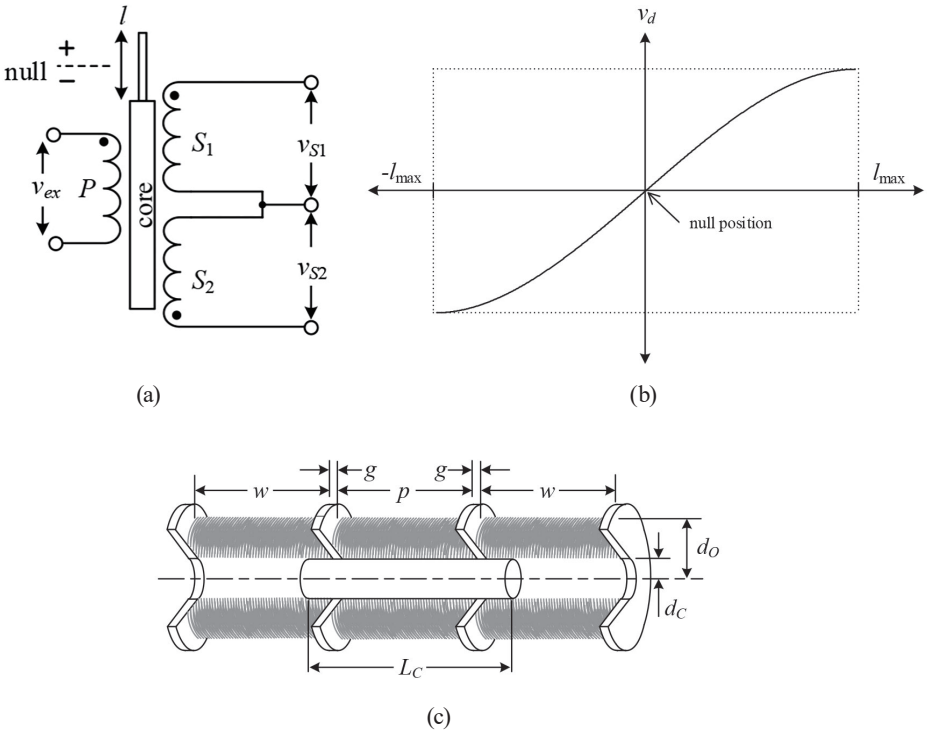

Fig. 1. (a) Principle, (b) output signal, and (c) structure of LVDT.

and ω_{ex} are the amplitude and frequency of the sinusoidal signal, respectively. If only the magnitude of the LVDT signal is considered, then the secondary winding signals v_{S1} and v_{S2} can be expressed as[12,22,23]

$$v_{S1} = \frac{2\pi^2 \omega_{ex} V_{ex} n_P n_S (2l_2 + p)}{10^7 w L_C Z_P \ln(d_O / d_C)} l_1^2, \tag{1a}$$

and

$$v_{S2} = \frac{2\pi^2 \omega_{ex} V_{ex} n_P n_S (2l_1 + p)}{10^7 w L_C Z_P \ln(d_O / d_C)} l_2^2, \tag{1b}$$

where Z_P denotes the impedance of the primary winding, and l_1 and l_2 are the lengths of the core penetrating into the secondary windings S_1 and S_2, respectively. From the structure of the LVDT, the displacement signal can be obtained from the difference signal between two secondary winding signals, $v_d = (v_{S1} - v_{S2})$, and can be stated as

$$v_d = K_1 l (1 - K_2 l^2), \tag{2}$$

for $K_1 = \dfrac{8\pi^2 \omega_{ex} V_{ex} n_P n_S (p + 2g + l_0) l_0}{10^7 w L_C Z_P \ln(d_O / d_C)}$, and $K_2 = \dfrac{1}{(p + 2g + l_0) l_0}$, where $l_0 = (l_1 + l_2)/2$ is the average length of the core penetrating into the secondary windings S_1 and S_2, and $l = (l_1 - l_2)/2$ is the core position. Practically, the length p is larger than the gap g or $p >> g$. From Fig. 1(c), the length L_C can be approximated as $L_C = 3p$; then, the difference signal v_d of Eq. (2) can be given by[4,12,24]

$$v_d = \frac{8\pi^2 \omega_{ex} V_{ex} n_P n_S}{10^7 Z_P \ln(d_O / d_C)} \frac{2p}{3w} \left(l - \frac{l^3}{2p^2} \right) = k_t l (1 - k_n l^2) , \tag{3}$$

where k_t and k_n are the sensitivity and nonlinear coefficient of the LVDT, respectively. The difference signal v_d of Eq. (3) exhibits only the amplitude of the AMSC from the LVDT output signal versus the excitation signal. To extract the displacement signal from the LVDT output signal, the synchronous demodulator is required to generate the envelope of the difference signal v_d. Note that the response of the demodulated signal is nonlinear along the entire core position, as shown in Fig. 1(b). The linear range of the LVDT transfer characteristic lies in a narrow range close to the zero crossing of the LVDT response curve. The LVDT signal v_d can be approximated as linear for the moving core varying in the narrow range close to the zero crossing of the LVDT transfer characteristic curve in Fig. 1(b). Thus, the difference signal v_d can be expressed as being in linear proportion to the core position l as

$$v_d = k_t l. \tag{4}$$

From Eqs. (2) and (3), the linear range defined by l_L of Eq. (4) is limited by the nonlinear coefficient k_n. Practically, the nonlinear coefficient k_n is described in terms of the acceptable error ε_L of the LVDT output signal. Therefore, the linear range l_L can be expressed as [23]

$$l_L = \pm \sqrt{\frac{\varepsilon_L}{k_n}} . \tag{5}$$

From the specifications of the LVDT used in this work, the acceptable error ε_L is equal to 0.5% and $k_n = 1.106 \times 10^{-3}$ V/mm^2; then, the linear range l_L is about ±2.13 mm.

3. Proposed Technique

The nonlinear term in parentheses in Eq. (3) causes the narrow linear operating range of the LVDT. This nonlinear term can be compensated using the inverse property $N(l)$ to extend the linear operating range as

$$N(l) = \frac{1}{(1 - \alpha v_d^2)} , \tag{6}$$

where α is the weighting coefficient used to minimize the error of the displacement signal. Practically, the magnitude of the term $k_n l^2$ in Eq. (3) is $|k_n l^2| < 1$. This is because the nonlinear coefficient k_n of a commercial LVDT is very small and unaffected when the displacement l approaches zero. Consequently, the weighting coefficient α in Eq. (6) is $\alpha < 1$. If the maximum value of the displacement signal v_d is assigned for the condition of $|\alpha v_d^2| < 1$, then Eq. (6) can be expanded using the binomial series as [24]

$$N(l) = 1 + \alpha v_d^2 + (\alpha v_d^2)^2 + (\alpha v_d^2)^3 + \cdots . \tag{7}$$

From Eq. (7), the higher order terms can be neglected when $|\alpha v_d^2| < 1$. Then, the nonlinear term $N(l)$ can be approximated as

$$N(l) = 1 + \alpha v_d^2 . \tag{8}$$

From Eq. (3), the nonlinear term $(1 - k_n l^2)$ can be compensated by the term $N(l)$ of Eq. (7). The block diagram for the linearization of the LVDT behavior is shown in Fig. 2(a). From Fig. 2(a), the output signal v_{ol} versus the signal v_d can be stated as

$$v_{ol} = v_d + \alpha v_d^3 = v_d (1 + \alpha v_d^2) . \tag{9}$$

From Eq. (9), if the displacement signal v_d is applied, the output signal v_{ol} can be given by

$$v_{ol} = k_t l + \left[(\alpha k_t^3 - k_t k_n) l^3 - 3\alpha k_t^3 k_n l^5 + 3\alpha k_t^3 k_n^2 l^7 - \alpha k_t^3 k_n^3 l^9 \right]. \tag{10}$$

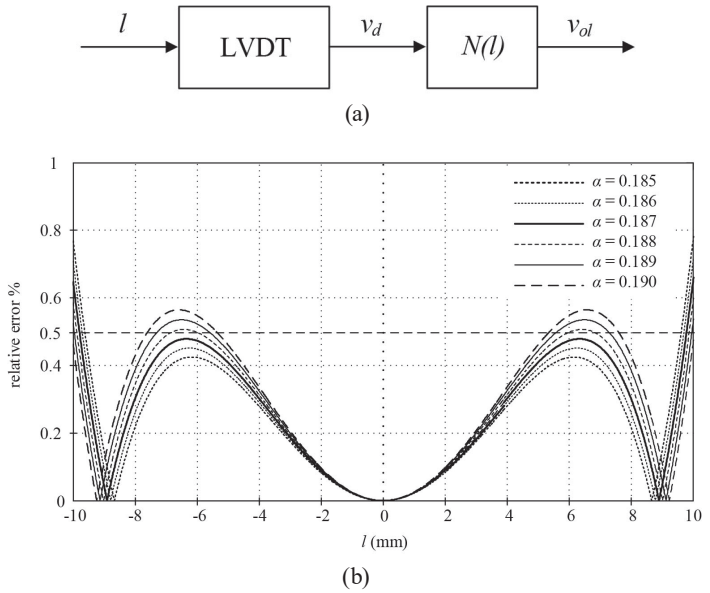

Fig. 2. (a) Principle of LVDT. (b) Plot of Eq. (12).

If an appropriate value of the weighting coefficient α is chosen, then the output signal v_{ol} in Eq. (10) can be approximated as

$$v_{ol} = k_t l \,. \tag{11}$$

The relative error of the output signal v_{ol}, defined by ε_{ol}, can be expressed as

$$\varepsilon_{ol} = \left[(\alpha k_t^2 - k_n) l^2 - 3\alpha k_t^2 k_n l^4 + 3\alpha k_t^2 k_n^2 l^6 - \alpha k_t^2 k_n^3 l^8 \right] \times 100\% \,. \tag{12}$$

The plot of Eq. (12) is shown in Fig. 2(b) and used to determine the coefficient α. From Fig. 2(b), if the relative error ε_{ol} of about 0.5% is assigned to equal the specification of the LVDT used in this work with the linear stroke range of about ±1.9 mm, then the weighting coefficient $\alpha = 0.187$ is observed at the core position $l = \pm 9.8$ mm. Note that the linear stroke range can be extended from ±1.9 to ±9.8 mm. The circuit diagram containing the property of Eq. (9) can be simply implemented using the analog multipliers and summing amplifier, as shown in Fig. 3(a). Note that the commercial analog multiplier provides an attenuation factor η. The summing amplifier comprises an operational amplifier (opamp), resistors R_1–R_3, and variable resistor R_n, as shown inside the dashed-line block in Fig. 3(a). Therefore, the output signal v_{ol} in Fig. 3(a) can be given by

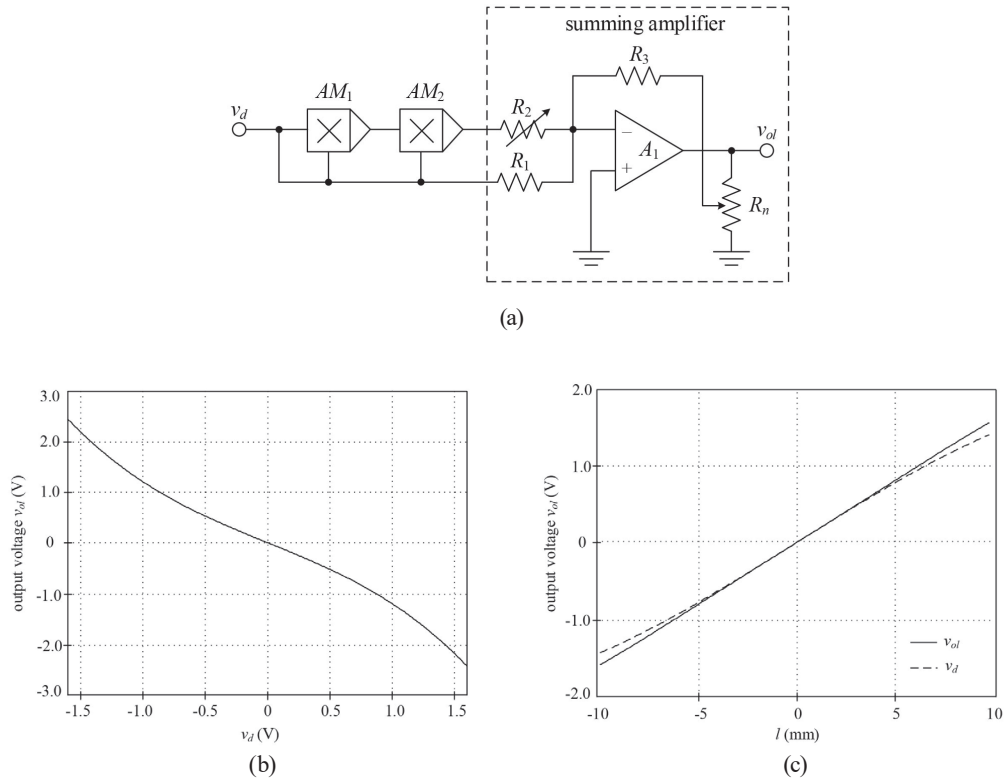

Fig. 3. (a) Proposed circuit, (b) simulation result of reverse transfer characteristic, and (c) linearization of LVDT.

$$v_{ol} = -\frac{R_3}{\beta R_1}\left(1+\frac{R_1}{R_2}\eta v_d^2\right)v_d\,, \tag{13}$$

where β is the amplification factor used to span the output signal v_{ol} to the appropriate value and to compensate nonideal values between resistors R_3 and R_1. Note that the output signal v_{ol} of the scheme in Fig. 3(a) is 180° out of phase. The parameters of the LVDT used in this work are measured from the experimental implementation as k_t = 84.817 mV/mm/V, k_n = 1.106 × 10^{-3} mm^{-2}, and l_L = ±1.9 mm for the relative error of 0.5%. The parameter k_n can be calculated from a maximum value of the transfer characteristic curve of the LVDT and Eq. (3) as

$$k_n = \frac{k_t l_m - v_{dm}}{k_t l_m^3}\,, \tag{14}$$

where v_{dm} and l_m are the maximum value of the LVDT transfer characteristic curve and the position along the length of the moving core at the maximum voltage v_{dm}, respectively. Simulation results of the LVDT reverse transfer characteristic in Fig. 3(b) and the linearization of the LVDT behavior using the proposed technique for an excitation signal with the peak amplitude of 1 V in Fig. 3(c) were obtained using the PSPICE analog simulation program. It can be seen that the linear operating range of the LVDT used in this study can be extended more than fivefold.

4. Performance of Proposed Scheme

Deviation from the ideal performance of the proposed scheme is caused by the nonideal characteristics of the analog multipliers and the tolerance of the resistors used in the summing amplifier. From Fig. 3(a), the output signal v_{ol} caused by the errors of the analog multipliers and the nonideal factor between the resistors R_1 and R_2, defined as Δ_{12}, can be expressed as

$$v_{ol} = -\frac{R_3}{\beta R_1}v_d\left(1+\frac{R_1}{R_2}\eta v_d^2\right)-\left(\Delta_{12}+\varepsilon_{m12}\right)\frac{R_3}{\beta R_2}\eta v_d^3\,, \tag{15}$$

where ε_{m12} denotes the error of the analog multipliers. From Eq. (15), the amplification factor β can be varied to assign the term $(R_3/\beta R_1) = K_L$, where K_L is the gain of the proposed scheme. Therefore, Eq. (15) can be rewritten as

$$v_{ol} = -K_L v_d\left(1+\frac{R_1}{R_2}\eta v_d^2\right)-\left(\Delta_{12}+\varepsilon_{m12}\right)K_L\frac{R_1}{R_2}\eta v_d^3\,. \tag{16}$$

From Eq. (16), the second term on the right-hand side, that is, the error term, can be minimized by replacing the resistor R_2 with the variable resistor. If the resistance R_2 is varied

to approach the expected value, then the relative error of the output signal v_{ol}, defined as ε_{oc}, can be expressed as

$$\varepsilon_{oc} = \frac{\eta R_1(\Delta_{12} + \varepsilon_{m12})v_d^2}{R_2\left(1 + \frac{R_1}{R_2}\eta v_d^2\right)} \times 100\% . \tag{17}$$

If the resistances R_1 and R_2 are chosen to satisfy the nonideal factor Δ_{12} of about 0.2%, error ε_{m12} = 0.4%, ($\eta R_1/R_2$) = 0.187, and the peak amplitude of the signal v_d = 762.97 mV corresponding to the core displacement l = 9.8 mm, then the relative error ε_{oc} of about 0.06% is calculated. Note that the relative error ε_{oc} is very small. Therefore, the inaccuracy of the proposed technique corresponding to the relative error ε_{oc} can be neglected. From Eqs. (12) and (17), it can be seen that the major factor contributing to the inaccuracy of the proposed technique is the relative error ε_{ol}.

5. Experimental Results

The proposed scheme in Fig. 3(a) was constructed using commercially available devices to demonstrate its performance, as shown in Fig. 4(a). The active devices used in this study were the analog multiplier AD633 and opamp LF351. The analog multiplier AD633 provides an attenuation factor of about 0.1. Therefore, η = 0.01 was obtained. The resistors $R_1 = R_3 = 20$ kΩ with 0.2% tolerance were chosen. From Eq. (12) and Fig. 2(b), $\eta R_1/R_2$ was equal to 0.187. Thus, the resistance R_2 was calculated as 10.7 kΩ. The resistor R_2 was replaced by the variable resistor to tune the resistance to be close to the calculated value. The variable resistor R_n of 1 kΩ was chosen. The power supply was set as ±9 V. The nonlinearity error of the term $v_d{}^2$ was measured to be about 0.4% or $\varepsilon_{m12} = 4 \times 10^{-3}$. The commercially available LVDT used in this study provides the following specifications: linear stroke range of ±2 mm, maximum relative error of 0.5%, and sensitivity k_t = 94.5 mV/mm/V. The excitation signal applied to

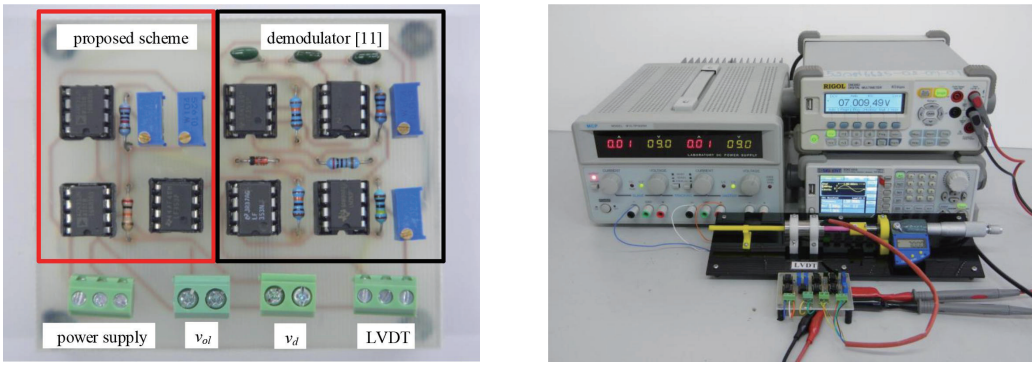

(a) (b)

Fig. 4. (Color online) (a) Proposed circuit. (b) Experimental setup.

the LVDT is set as a 2.5 kHz sinusoidal wave with a 2 V peak-to-peak amplitude. In this experiment, the output signal of the LVDT is demodulated using the technique proposed in the literature[13]. The experimental setup is shown in Fig. 4(b). The practical behavior of the LVDT is measured and shown in Fig. 5 to extract the parameters. The parameters of the LVDT can be determined as follows. The sensitivity of the LVDT is determined to be 84.817 mV/mm/V.

The maximum amplitude of the LVDT signal v_{dm} is 971.55 mV at the maximum stroke or $l_m = \pm 16$ mm, and the linear range of the LVDT is about ±1.9 mm for the relative error of 0.5%. The nonlinear coefficient k_n can be calculated using Eq. (14) as 1.106×10^{-3} V/mm^2. The LVDT inverse transfer characteristic of the proposed scheme is shown in Fig. 6(a), where the difference signal v_d is assigned as $(v_{s2} - v_{s1})$ or $-v_d$ for the inverse operation of the signal v_{ol}. The demodulated LVDT signal is synthesized using the LabVIEW program and analog input/output board from National Instruments (NI-USB-6009) to demonstrate the performance of the proposed technique, where the LVDT parameters are set to the same parameters as the practical LVDT used in this study. The synthesized signal is applied to the scheme in Fig. 3(a) for the peak amplitude of ±971.55 mV corresponding to the core position of ±16 mm. The measured

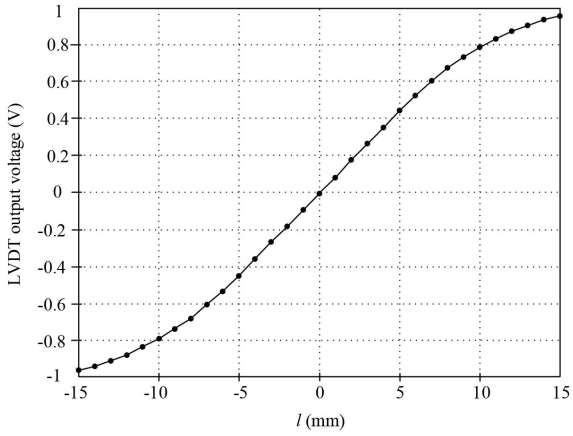

Fig. 5. Practical behavior of LVDT.

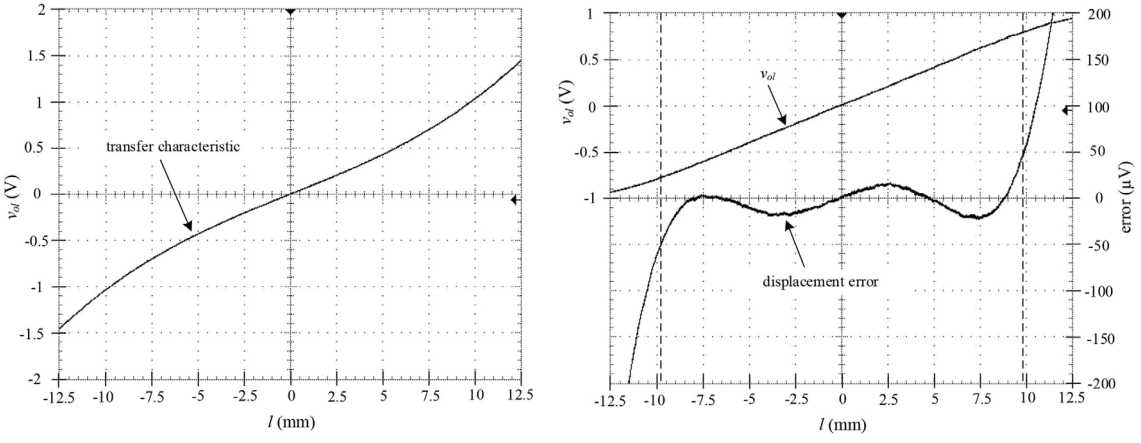

Fig. 6. (a) Transfer characteristic of the proposed scheme. (b) Measured result of the proposed scheme.

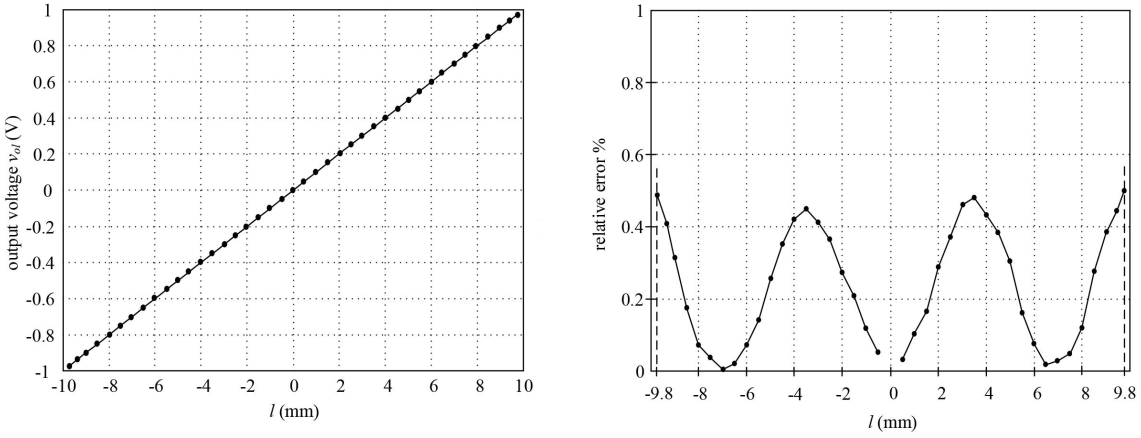

(a) (b)

Fig. 7. (a) Measured result of the output signal. (b) Relative error.

result confirmed the proposed technique performance, as shown in Fig. 6(b). It can be seen that the proposed technique can extend the linear operating range from ±1.9 to ±9.8 mm. Figure 7(a) shows the plot of the average voltage of the output signal v_{ol} from the circuit in Fig. 3(a) of 5 repeated measurements for each core position from –9.8 to 9.8 mm. The sensitivity of the proposed scheme is set to 100 mV/mm/V by adjusting the variable resistor R_n to vary the amplification factor β. The relative error ε_r of the measured signal v_{ol} is shown in Fig. 7(b). The maximum relative error ε_r of the measured result in Fig. 7(b) corresponding to the absolute error ε_{am} of about 46 μm is observed, where the maximum relative error ε_r occurs at the core position of ±9.8 mm. The full-scale error of the proposed technique, defined as ε_{fs}, can be stated as

$$\varepsilon_{fs} = \frac{\max(\varepsilon_{am})}{\left|\max(stroke\ \ range)\right|} \times 100\% . \tag{18}$$

If the maximum absolute error ε_{am} is equal to 46 μm, the full-scale error ε_{fs} is calculated to be about 0.23%.

6. Conclusions

The inverse transfer characteristic of an LVDT based on a binomial series was proposed in this paper. A simple circuit configuration comprising analog multipliers and an opamp was adopted for synthesizing the LVDT inverse transfer characteristic without a specific device. The linear operating range of the LVDT was extended more than fivefold from the LVDT specification used in this study, that is, from ±1.9 to ±9.8 mm. The performance of the proposed circuit was confirmed by experimental implementation. The proposed circuit can be used as a signal conditioner to measure a large displacement using a small-structure LVDT with very good performance. The proposed technique exhibits a simple configuration that is suitable for measurement systems used in small areas such as a miniature robot and an embedded system.

Acknowledgments

This work was supported by the King Mongkut's Institute of Technology Ladkrabang (KMITL), Thailand, under Grant KREF115701.

References

1 R. Pallas-Areny and J. G. Webster: Sensor and Signal Condition (John Wiley & Sons, New York, 2001) p. 229.
2 K. Ara: IEEE Trans. Instrum. Meas. **21** (1972) 249. https://doi.org/10.1109/TIM.1972.4314011
3 S. C. Saxena and S. B. L. Seksena: IEEE Trans. Inst. Meas. **38** (1989) 748. https://doi.org/10.1109/19.32186
4 H. K. P. Neubert: Instrument Transducers - An Introduction to Their Performance and Design (Oxford, New York, 1975) p. 204.
5 S. Cetinkunt: Mechatronics (John Wiley & Sons, New York, 2006) p. 227.
6 M. Felix, A. Lizarraga, A. Islas, and A. Gonzales: 36th Annual Conf. IEEE Industrial Electronics Society (2010) 1772.
7 R. M. Ford, R. S. Weissbach, and D. R. Loker: 17th IEEE Instrumentation and Measurement Technology Conf. (IMTC/2000) 1448.
8 S. Lee and W. Kim: IEEE Trans. Control Syst. Tech. **18** (2010) 859. https://doi.org/10.1109/TCST.2009.2030413
9 G. Chen, B. Zhang, P. Liu, and H. Ding: IEEE Sens. J. **15** (2015) 2248. https://doi.org/10.1109/JSEN.2014.2364610
10 W. Petchmaneelumka, A. Rerkratn, A. Luangpol, and V. Riewruja: J. Circ. Syst. Comp. **27** (2018) 1850182. https://doi.org/10.1142/S0218126618501827
11 W. Petchmaneelumka, P. Mano, and V. Riewruja: Sens. Mater. **30** (2018) 2171. https://doi.org/10.18494/SAM.2018.1816
12 P. Veeraian, U. Gandhi, and U. Mangalanathan: Int. J. Electron. Commun. **79** (2017) 141. https://doi.org/10.1016/j.aeue.2017.05.037
13 W. Petchmaneelumka, K. Songsuwankit, and V. Riewruja: I.R.E.E. **11** (2016) 340. https://doi.org/10.15866/iree.v11i3.8906
14 W. Petchmaneelumka, P. Mano, K. Songsuwankit, and V. Riewruja: Int. J. Electron. **105** (2018) 1520. https://doi.org/10.1080/00207217.2018.1461250
15 V. Riewruja and T. Kamsri: IET Circ. Device Syst. **3** (2009) 57. https://doi.org/10.1049/iet-cds.2008.0140
16 V. Riewruja and A. Rerkratn: Int. J. Electron. **98** (2011) 459.
17 V. Riewruja and A. Rerkratn: Indian J. Pure Appl. Phys. **48** (2010) 67.
18 A. Drumea, A. Vasile, M. Comes, and M. Blejan: 1st Electronics System Integration Technology Conference (2006) 629.
19 K. Banerjee, B. Dam, and K. Majumdar: IEEE Int. Symp. Industrial Electronics (2013) 1. https://doi.org/10.1109/ISIE.2013.6563715
20 R. Casanella, O. Casas, and R. Pallas-Areny: Meas. Sci. Technol. **16** (2005) 1637. https://doi.org/10.1088/0957-0233/16/8/014.
21 R. Casanella, O. Casas, M. Ferrari, V. Ferrari, and R. Pallas-Areny: IEEE Trans. Instrum. Meas. **56** (2007) 1219. https://doi.org/10.1109/TIM.2007.899919.
22 S. R. Mishra, G. Panda, and D. P. Das: IEEE Trans. Instrum. Meas. **59** (2010) 947. https://doi.org/10.1109/TIM.2009.2031385.
23 W. Petchmaneelumka, W. Koodtalang, and V. Riewruja : IEEE Sensors J. **19** (2019) 5045. https://doi.org/10.1109/JSEN.2019.2902879
24 M. R. Spiegel: Mathematical Handbook (Scaum's Outline Series, Singapore, 1968) p. 110.